Medical Engineering and Physics 63 (2019) 42–49

Contents lists available at ScienceDirect

Medical Engineering and Physics

journal homepage: www.elsevier.com/locate/medengphy

Modeling left ventricular dynamics using a switched system approach based on a modified atrioventricular piston unit

Huan Huang[a], Zhan Shu[a,b,*], Bo Song[a], Liya Ji[c], Nan Zhu[a]

[a] School of Electrical Engineering and Automation, Jiangsu Normal University, Xuzhou, Jiangsu, China
[b] Electro-Mechanical Group, Faculty of Engineering and the Environment, University of Southampton, Southampton SO17 1BJ, UK
[c] Department of Cardiology, Xuzhou Central Hospital, Xuzhou, Jiangsu, China

ARTICLE INFO

Article history:
Received 9 August 2018
Revised 26 November 2018
Accepted 4 December 2018

Keywords:
Lumped-element ventricular model
Switched system
Atrioventricular plane displacement
End-systolic pressure volume relationship
Ventricular compliance

ABSTRACT

The contribution of the longitudinal atrioventricular plane displacement to ventricular pumping has drawn more and more attentions. In this paper, differential equations of the left ventricle (LV) are derived *via* the atrioventricular piston concept. The contribution of left ventricular radial function to blood flow was converted to an equivalent coefficient. A systemic circulatory model incorporating the modified atrioventricular piston unit was developed on a switched system form by adding some state-dependent switching planes. Simulation results prove that the end-systolic pressure volume relationship of the model with a changing systemic arterial resistance is approximately linear and insensitive to perturbations in afterload. Then the LV model was validated using a data fitting method. A pressure–volume loop from a patient undergoing routine diagnostic cardiac catheterization with LV angiography was used as measurements. Model parameters and the trapezoidal profile of contraction forces were adjusted by a trial method. The root mean squared error between the measured and estimated LV pressure is 2.99 mmHg. The LV compliance is 0.34 ml/mmHg. The ratio between left ventricular and left atrial cross-section is 1.8. Therefore, parameter values used in the modified LV model match physiological data. The model can reproduce the realistic pressure-flow relationship in the LV chamber.

© 2018 IPEM. Published by Elsevier Ltd. All rights reserved.

1. Introduction

Patient-specific heart models have become increasingly powerful to improve diagnosis and predict therapeutic effects. Although great advances have been made to develop the three-dimensional finite element models [1,2], lumped-element models are important tools for characterizing the global function of heart and constructing multiscale models [3].

Since the experiments of Suga et al. [4,5], the concept of time-varying elastance has been extensively used in cardiovascular system simulation and left ventricular assist device design [6,7]. The model uses a time-varying elastance to represent the pressure–volume (PV) relationship in heart chambers. Although the end-systolic pressure–volume relationship (ESPVR) of the left ventricle (LV) can be achieved by an elastance curve, the model cannot explain the behavior of ventricular walls and fails to simulate the ventricular function when there is an interaction between the LV and an assist device [8,9].

In order to accurately characterize cardiac functions, a variety of myofiber models have been developed [8,10,11] to replace the elastance model. If the anatomic coupling between left and right ventricles is considered, a whole-heart model can be achieved based on a sarcomere mechanics component [12]. Although these models have been applied to heart geometry prediction [13] and cardiac resynchronization therapy [14], a great number of nonlinear equations and parameters in them limit the application of system identification and control techniques.

The ventricular pump mechanics is traditionally attributed to the radial squeezing of ventricular walls with considerable changes in epicardial volume throughout the cardiac cycle. However, MR images and finite element simulations show that the atrioventricular plane can slide along the pericardium with a restricted volume change of the total heart [15,16], resulting in the back-and-forth longitudinal movement of the atrioventricular plane in the base-apex direction. Furthermore, the atrioventricular plane displacement (AVPD) is a valuable indicator in clinical studies [17,18]. A reduced AVPD is strongly related to heart failure [19]. More

Abbreviations: PV, Pressure volume; ESPVR, End-systolic pressure volume relationship; LV, Left ventricle; LA, Left atrium; AVPD, Atrioventricular plane displacement; AVP, Atrioventricular piston; VC, Ventricular contraction; VR, Ventricular relaxation; AC, Atrial contraction; ABP, Arterial blood pressure; RMSE, Root mean squared error.

* Corresponding author at: Electro-Mechanical Group, Faculty of Engineering and the Environment, University of Southampton, Southampton SO17 1BJ, UK.
E-mail address: Z.Shu@soton.ac.uk (Z. Shu).

https://doi.org/10.1016/j.medengphy.2018.12.007
1350-4533/© 2018 IPEM. Published by Elsevier Ltd. All rights reserved.

recently, the AVPD is considered as a major contributor to ventricular pumping in healthy adults [20,21], accounting for 60% and 80% of the left and right ventricular stroke volume, respectively.

Through the longitudinal AVPD, the atrioventricular interaction can be established with the atrioventricular plane functioning as a piston unit. Experimental studies have shown that the piston-like structure is crucial to aiding the LV diastolic filling [22,23]. Based on the concept, an atrioventricular piston (AVP) model was developed by a bond-graph method [24]. Compared with the elastance model, the AVP model is able to generate the normal pattern of mitral flow. There is strong evidence to support the model insofar as the atrioventricular plane velocity profile reproduced by the model has a similar pattern compared with the realistic one measured by the Tissue Velocity Imaging.

The AVP model mainly focuses on the effect of longitudinal AVPD. However, Magnetic Resonance Imaging have revealed that the stroke volume due to radial shortening cannot be ignored [21]. In order to improve modeling accuracy, the radial motion of ventricular walls should be considered. In the original AVP model [24], because the dwell time of contraction forces was manually determined, it is difficult to ensure the piston unit moves back to its initial position after multiple cardiac cycles. Some variables, e.g., the LV volume and AVPD, cannot converge. To solve these problems, a switched system approach is proposed to modify the AVP model.

The nonlinearity of heart is strongly related to its switching properties. The open and closed states of valves divide the cardiovascular system into several subsystems. The alternate ventricular and atrial contraction forces lead to a periodic movement of atrioventricular plane. In this paper, the contribution of radial function is incorporated into a modified piston unit. Then the systemic circulatory model is converted to a switched system form by adding some state-dependent switching laws so that all the state variables converge to a limit cycle [25,26]. Related theories about the switched system [27,28] have laid a firm foundation for its applications in cardiovascular system analysis and ventricular assist device control.

In the AVP model, some parameter values, e.g., the LV compliance and the amplitude of contraction forces, haven't been clinically validated due to the fact that direct measurements are often not achievable. In our study, a PV loop from a patient was used to validate the model by a data fitting method. The ESPVR of the model was studied using simulation data. This paper provides a novel approach to model the systemic circulatory system. Parameters in the modified AVP model can help us understand the LV function.

2. Methods

2.1. Description of the AVP model

The AVPD of left heart is illustrated in Fig. 1. The AVP slides along the pericardium derived by the contraction force F_C which consists of the ventricular contraction force F_{VC} and the atrial contraction force F_{AC}. During ventricular contraction (VC), the AVP is pulled towards the apex by F_{VC}, ejecting blood into arteries through the aortic valve. During ventricular relaxation (VR), F_C is equal to zero and the AVP moves towards the opposite direction by means of a hydraulic force, causing a redistribution of blood from the left atrium (LA) into the LV through the mitral valve [24]. During atrial contraction (AC), F_{AC} arises and aids the ventricular filling until the start of F_{VC}. The stroke length of AVP is defined to be the distance from end diastole to end systole.

Fig. 2 shows a schematic illustration of the AVP model. The left heart is equivalent to a piston pump where the ventricular and atrial chambers have a constant cross-section and a hollow piston

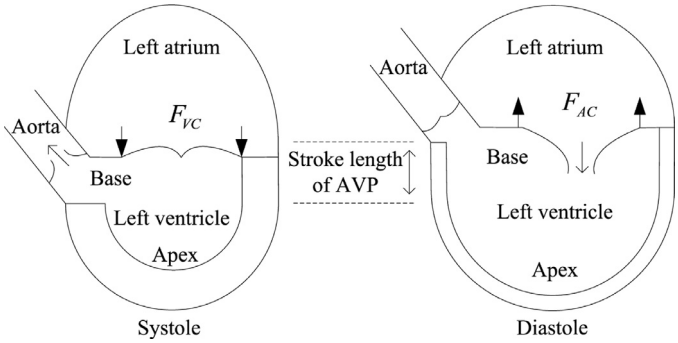

Fig. 1. The AVPD of left heart. The AVP is rigidly connected to the mitral and aortic valve. During systole, the AVP is pulled towards apex by F_{VC} with myocardial shortening. During diastole, the AVP moves back by means of F_{AC} and a hydraulic force.

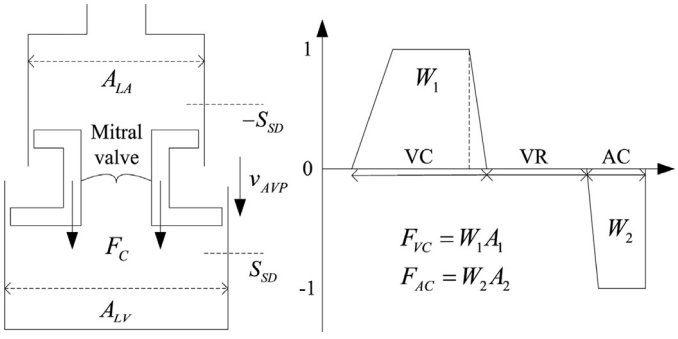

Fig. 2. Schematic illustration of the AVP model without epicardial volume changes. F_C consists of the ventricular contraction force F_{VC} and the atrial contraction force F_{AC}. Trapezoidal windows W_1 and W_2 define the profile of F_{VC} and F_{AC}, respectively. A_1 and A_2 are their amplitude.

placed in between [23]. The piston slides along the longitudinal direction. The myocardial force follows a trapezoidal profile. W_1 and W_2 are two normalized trapezoidal windows, representing the profile of F_{VC} and F_{AC}, respectively. Because the atrial repolarization wave (Ta wave) is usually hidden in the QRS complex, the start of W_1 is set to be the end of W_2 which is a right-angled trapezoid. There are total six free vertices in W_1 and W_2. The amplitude of F_{VC} and F_{AC} is defined as A_1 and A_2, respectively. One cardiac cycle is divided into three phases by F_C. During VC, VR and AC, F_C is equal to W_1A_1 (F_{VC}), zero and W_2A_2 (F_{AC}), respectively.

In the longitudinal direction, the dynamics of AVP can be modeled as

$$\begin{aligned} &L_{AVP}\dot{v}_{AVP} + R_{AVP}v_{AVP} + P_{LV}A_{LV} - P_{LA}A_{LA} = F_C \\ &\dot{s}_{AVP} = v_{AVP}, \end{aligned} \tag{1}$$

where v_{AVP} denotes the velocity of AVP and s_{AVP} denotes the AVPD. A_{LV} and A_{LA} are defined as the largest epicardial short-axis area of the LV and LA, respectively [21]. The difference between A_{LV} and A_{LA} is crucial to ventricular filling [23]. P_{LV} and P_{LA} denote the LV and LA pressure, respectively. L_{AVP} and R_{AVP} denote the inertia and damping of AVP, respectively. The model characterizes the atrioventricular interaction between P_{LV}, P_{LA} and F_C.

2.2. Construction of the switched systemic circulatory model

In this section, the systemic circulation is modeled in a switched system context. State-dependent switching planes are introduced to ensure the convergence of state variables. Definitions about switched systems are presented in Appendix A.

Electrical analogs of the systemic circulatory model are displayed in Fig. 3. The model uses two diodes with forward resis-

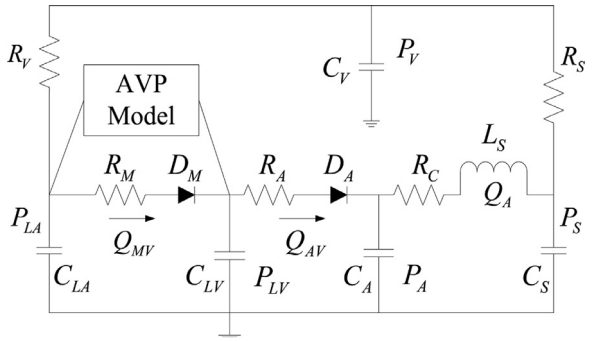

Fig. 3. Electrical analogs of the systemic circulatory model. P_{LV}: left ventricular pressure; P_A: aortic pressure; Q_A: aortic flow; P_S: systemic arterial pressure; P_V: venous pressure; P_{LA}: left atrial pressure, Q_{MV}: mitral valve flow, Q_{AV}: aortic valve flow, Q_{MV} - $Q_{AV} = Q_{LV}$: left ventricular flow. Model parameters are listed in Table 1.

tance as aortic (D_A and R_A) and mitral (D_M and R_M) valves and a five-element vascular model [6] (C_A, R_C, L_S, C_S, R_S) as arteries. C_V and R_V denote venous compliance and resistance, respectively. The passive compliance of ventricular and atrial chambers is represented by two capacitors, i.e., the LV capacitor (C_{LV}) and the LA capacitor (C_{LA}). The AVP model is connected between them according to the atrioventricular interaction relationship.

The state vector of the system is defined to be

$$x = \begin{bmatrix} P_{LV} & P_A & Q_A & P_S & P_V & P_{LA} & v_{AVP} & s_{AVP} \end{bmatrix}^T.$$

One normal cardiac cycle is usually divided into four basic phases according to the open/closed (O/C) state of D_A and D_M, namely ejection, isovolumic relaxation, filling and isovolumic contraction. Additionally, the switch of F_C should also be entailed. As a result, one cardiac cycle is further divided into seven subsystems in the sequence of (O C F_{VC}), (O C 0), (C C 0), (C O 0), (C O F_{AC}), (C O F_{VC}), (C C F_{VC}), using the state set of (D_A D_M F_C) as an indicator. Here it assumes that F_{VC} falls rapidly to zero before the isovolumic relaxation phase (C C 0). A switch between the ith and jth subsystem occurs when the state vector reaches a switching plane, see (A.3). Corresponding to the seven subsystems, switching planes should satisfy the following rules

$$\begin{aligned}
\tilde{c}_{12} &= \begin{bmatrix} 0 & 0 & 0 & 0 & 0 & 0 & 0 & 1 & -S_{SD} \end{bmatrix}^T \\
\tilde{c}_{23} &= \begin{bmatrix} 1 & -1 & 0 & 0 & 0 & 0 & 0 & 0 & 0 \end{bmatrix}^T \\
\tilde{c}_{34} &= \begin{bmatrix} 1 & 0 & 0 & 0 & 0 & -1 & 0 & 0 & 0 \end{bmatrix}^T \\
\tilde{c}_{45} &= \begin{bmatrix} 0 & 1 & 0 & 0 & 0 & 0 & 0 & 0 & -P_{ST} \end{bmatrix}^T \\
\tilde{c}_{56} &= \begin{bmatrix} 0 & 0 & 0 & 0 & 0 & 0 & 0 & 1 & S_{SD} \end{bmatrix}^T \\
\tilde{c}_{67} &= \begin{bmatrix} 1 & 0 & 0 & 0 & 0 & -1 & 0 & 0 & 0 \end{bmatrix}^T \\
\tilde{c}_{71} &= \begin{bmatrix} 1 & -1 & 0 & 0 & 0 & 0 & 0 & 0 & 0 \end{bmatrix}^T.
\end{aligned} \tag{2}$$

$\tilde{c}_{23}$, $\tilde{c}_{34}$, $\tilde{c}_{67}$ and $\tilde{c}_{71}$ indicate that a subsystem switches when the pressure gradient over valves is equal to zero. S_{SD} which has a positive value was used to limit the AVPD within a certain range, as shown in Fig. 2. When s_{AVP} reaches S_{SD} or -S_{SD}, the state of F_C changes. The distance between S_{SD} and -S_{SD} is slightly less than the stroke length of AVP because of the inertia of AVP.

Fig. 4 shows two arterial blood pressure signals recorded in the MIT MIMIC database [29,30] (mimic2wdb/31/30,000,038). For each cardiac cycle, the time of peak P wave in ECG was first marked. Then, at the time, corresponding arterial pressure value was recorded as P_{ST}. It can be seen that P_{ST} simultaneously fluctuates with arterial pressure. A larger oscillation in the upper arterial pressure waveform leads to a larger oscillation in the corresponding P_{ST} waveform. Therefore, the value of P_{ST} is related to mean

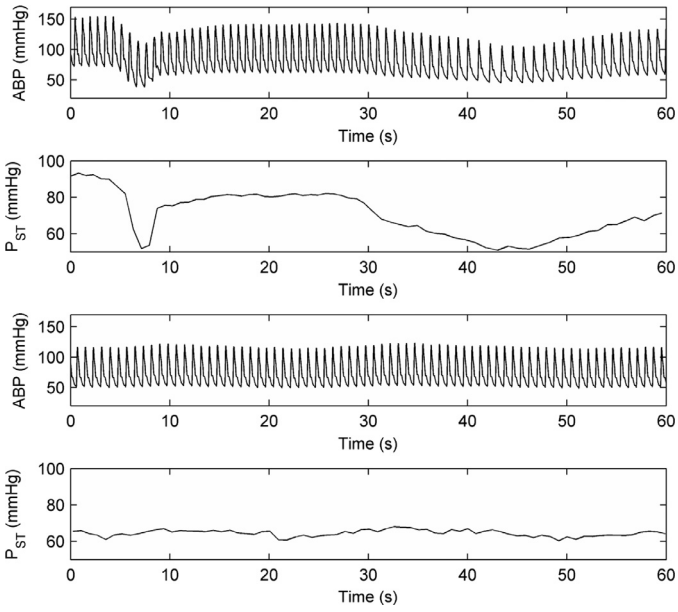

Fig. 4. The oscillation of P_{ST} for different arterial blood pressure (ABP) signals.

Table 1
Reference parameter values of the systemic circulatory model.

	Value	Description
R_C	0.05 mmHg s/ml	Characteristic resistance
R_S	1 mmHg s/ml	Systemic arterial resistance
L_S	0.001 mmHg s^2/ml	Arterial inertance
C_S	1.2 ml/mmHg	Systemic arterial compliance
C_A	0.08 ml/mmHg	Aortic sinus compliance
C_V	50 ml/mmHg	Venous compliance
R_A	0.005 mmHg s/ml	Aortic valve resistance
R_M	0.005 mmHg s/ml	Mitral valve resistance
C_{LV}	0.3 ml/mmHg	Left ventricular compliance
C_{LA}	0.3 ml/mmHg	Left atrial compliance
R_V	0.01 mmHg s/ml	Venous resistance
R_{AVP}	300 mmHg cm s	Damping of AVP
L_{AVP}	30 mmHg cm s^2	Inertia of AVP
A_1	5880 mmHg cm^2	Amplitude of F_{VC}
A_2	1200 mmHg cm^2	Amplitude of F_{AC}
A_{LV}	40 cm^2	Left ventricular cross-section
A_{LA}	20 cm^2	Left atrial cross-section
S_{SD}	0.7 cm	Switching distance for AVP
P_{ST}	90 mmHg	Switching threshold for AC
k_{RAD}	1.1	Radial function coefficient

blood pressure and heart rate. In order to simulate the function of P wave, $\tilde{c}_{45}$ was used to trigger AC, i.e., a switch between (C O 0) and (C O F_{AC}) occurs when P_A becomes smaller than P_{ST}. A larger P_{ST} will accelerate the heart rate.

Reference parameter values of the model are listed in Table 1. Compared with the original AVP model, A_{LV} and A_{LA} were set to a smaller value given by Maksuti et al. [23]. S_{SD} was set to 0.7 cm so that the stroke volume is about 90 ml. P_{ST} was adjusted to 90 mmHg to generate a mean arterial pressure of 100 mmHg and a cardiac output of 5.5 L/min. In simulations, F_{VC} and F_{AC} were set to a rectangular profile. The state space equations of each subsystem were derived using Kirchhoff's voltage and current laws and simulated in MATLAB.

2.3. Modeling the radial function

From Fig. 3, P_{LV} satisfies

$$\begin{aligned}
C_{LV}\dot{P}_{LV} &= Q_{MV} - Q_{AV} + A_{LV}v_{AVP} \\
&= Q_{LV} + A_{LV}v_{AVP}.
\end{aligned} \tag{3}$$

The total LV flow Q_{LV} is the sum of mitral valve flow Q_{MV} and aortic valve flow Q_{AV}. $A_{LV}\ v_{AVP}$ denotes the flow generated by the longitudinal motion of AVP. Taking the radial motion of ventricular walls into account, (3) can be modified to

$$C_{LV}\dot{P}_{LV} = Q_{LV} + (1 + k_{RAD})A_{LV}v_{AVP}, \tag{4}$$

where the LV radial function was converted to an equivalent coefficient k_{RAD} (see Appendix B). Since AVPD accounts for about 60% of stroke volume, the value of k_{RAD} in simulations was adjusted until the condition was satisfied. The contribution of AVPD is equal to A_{LV} multiplied by the stroke length of AVP.

2.4. Calculating the ESPVR

ESPVR is usually defined to be the maximal elastance ($E_{\max}$) at the end-systole by the following equation

$$E_{\max} = \max\left(\frac{P_{LV}(t)}{V_{LV}(t) - V_0}\right), \tag{5}$$

where V_0 is the LV volume (V_{LV}) at zero pressure over one cardiac cycle. $E_{\max}$ can be estimated by an iterative method [31,32]. Firstly, V_0 was fixed at zero and (5) was used to calculate the maximal PV point for each cardiac cycle. Then a linear least squares method was applied to yield the slope and intercept (V_0) estimates. With this new V_0 estimate, the process was repeated until convergence was achieved. In simulations, a set of PV loop was acquired by changing R_S. The sensitivity of ESPVR to perturbations in model parameters will be discussed.

2.5. Model validation

From (1) and (4), the LV model is

$$\begin{aligned}\dot{v}_{AVP} &= -\frac{R_{AVP}}{L_{AVP}}v_{AVP} - \frac{A_{LV}}{L_{AVP}}P_{LV} + \frac{A_{LA}}{L_{AVP}}P_{LA} + \frac{F_C}{L_{AVP}}\\ \dot{P}_{LV} &= \frac{(1 + k_{RAD})A_{LV}}{C_{LV}}v_{AVP} + \frac{1}{C_{LV}}Q_{LV}.\end{aligned} \tag{6}$$

The expression of F_C, i.e., W_1A_1, 0 or W_2A_2 depends on the state of cardiac phases. Although some parameters, e.g., A_{LV}, A_{LA} and k_{RAD}, are time-varying due to the switch of valves and the change of LV diameter, they were approximately set to be constant in our model. Model accuracy should be validated using realistic measurements.

The LV pressure (Fig. 5a) and volume (Fig. 5b) measurements were obtained from a patient (57 years of age, male) with coronary arterial stenosis. A 6F pigtail catheter was advanced across the aortic valve into the LV for pressure measurement and angiography. The peak R wave of ECG was used as an end-diastolic timing marker, as shown in Fig. 5a. Single plane angiocardiograms were recorded in the 30° right anterior oblique projection using a GE advantx LCV+system at 50 frames/s. V_{LV} was calculated *via* Simpson's algorithm. The sampling rate of V_{LV} measurements was doubled to 100 Hz by a piecewise linear interpolation method.

Parameter values of the model were validated using a data fitting method. The parameter vector θ is chosen as

$$[\theta_1\theta_2\theta_3\theta_4\theta_5\theta_6\theta_7] = \left[\frac{R_{AVP}}{L_{AVP}}\ \frac{A_{LV}}{L_{AVP}}\ \frac{A_{LA}}{L_{AVP}}\ \frac{(1 + k_{RAD})A_{LV}}{C_{LV}}\ \frac{1}{C_{LV}}\ \frac{A_1}{L_{AVP}}\ \frac{A_2}{L_{AVP}}\right]. \tag{7}$$

Q_{LV} and P_{LA} are used as input variables. Given Q_{LV}, P_{LA} and θ, the estimate of P_{LV}, i.e., $\hat{P}_{LV}$, can be solved from (6). The root mean squared error (RMSE) between P_{LV} and $\hat{P}_{LV}$ was used to evaluate the fitting accuracy. The Q_{LV} displayed in Fig. 5c was calculated by the time derivative of V_{LV}. In order to minimize the need for invasive sensors, P_{LA} was not clinically measured but approximated by the value of P_{LV} at the time of mitral valve opening or closing.

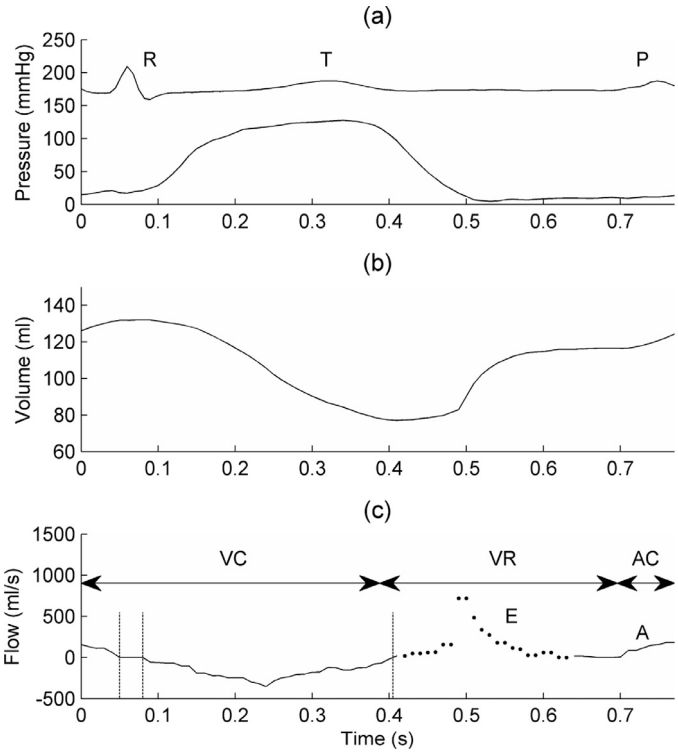

Fig. 5. The LV pressure (a) and volume (b) measurements from a patient. (c): Q_{LV} calculated from the LV volume was divided into three phases, i.e., VC, VR and AC. The time of aortic/mitral valve opening or closing is marked by vertical lines. The mitral flow has two peaks, i.e., E-wave (dotted line) and A-wave.

Trapezoidal F_{VC} and F_{AC} are required to ensure the data fitting accuracy. Firstly, positions of the six vertices in W_1 and W_2 should be determined. During AC, the A-wave of mitral flow increases from zero to its peak value. Hence the region of AC phase can be fixed by means of the flow waveform. Other four vertices were manually adjusted until the RMSE between P_{LV} and $\hat{P}_{LV}$ reaches a smaller value.

In the Q_{LV} waveform, the time of aortic/mitral valve opening or closing is marked by vertical lines where Q_{LV} is equal to zero. The time of mitral valve opening is not recorded, implying that the E-wave occurs earlier than expected. The measurement error is mainly due to the limitation of the angiography method which assumes the ventricle to be an ellipsoid. In reality, the ventricle has an irregular geometry and the deformation of ventricle varies between locations. In order to avoid serious deviation in $\hat{P}_{LV}$, the E-wave data (dotted line) was excluded from the data fitting procedure. In detail, the estimation errors between P_{LV} and $\hat{P}_{LV}$ over the E-wave region were set to zero, i.e., let $\hat{P}_{LV}$ equal to P_{LV}.

3. Results

Fig. 6 shows the simulated P_{LV}, V_{LV}, P_A, Q_{LV}, v_{AVP} and s_{AVP} by the modified AVP model. V_{LV} was calculated by the integration of Q_{LV} with 90 ml as an initial value. The value of k_{RAD} was set to 1.1, so that the contribution of AVPD is 60%~65% for all the simulations. For comparison, the simulated Q_{LV} was also divided into three phases. Dwell times of VC, VR and AC are not predetermined as in the original AVP model but depend on the switching rules (2).

Fig. 7 includes seven PV loop sets. In order to clearly compare their difference, in each PV loop, only the point corresponding to $E_{\max}$ is recorded. Set A (solid line) was obtained by increasing R_S over the interval [0.8, 1.6]. Set B (asterisk) was given by a smaller

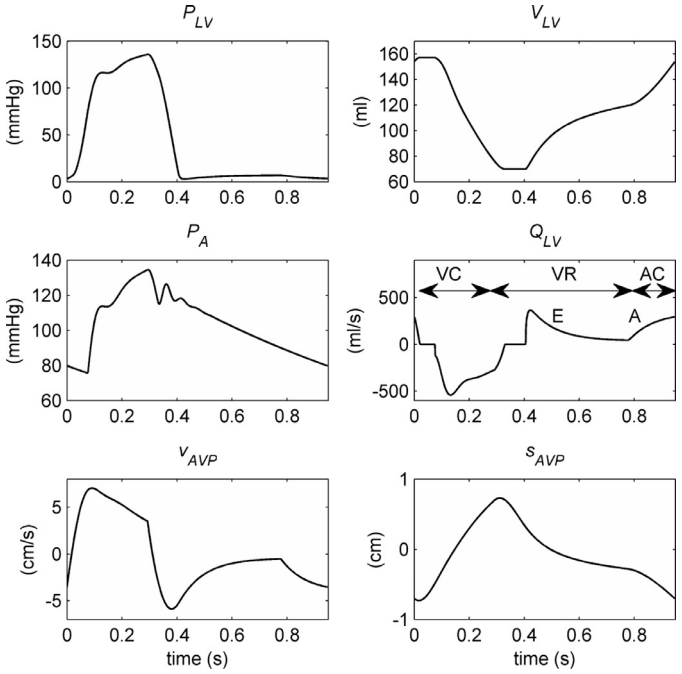

Fig. 6. Simulation results of the modified AVP model.

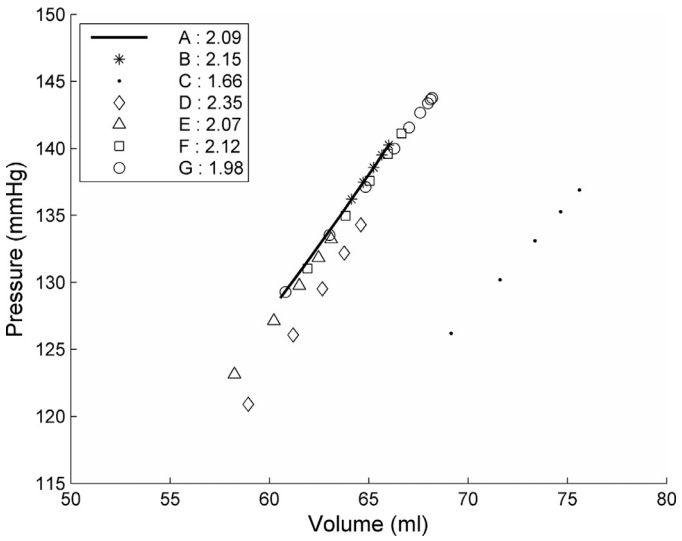

Fig. 7. ESPVRs of the seven PV loop sets (from Set A to Set G) obtained by increasing R_S. In each set, the PV points corresponding to E_{max} are recorded. Set A has a larger R_S changing range than Set B. From Set C to Set G, perturbations in different parameters are added, namely C_{LV} (C), R_{AVP} (D), C_S (E), R_C (F) and P_{ST} (G).

interval [1.2, 1.6]. Other sets exhibit the influence of parameter perturbations to ESPVR with R_S changing over [0.8, 1.6]. For each set, only a single parameter was disturbed while others were fixed at their reference values. In set C (dot) and D (diamond), two LV parameters, i.e., C_{LV} and R_{AVP}, were increased by 30%. In set E (triangle) and F (square), two vascular parameters, i.e., C_S and R_C, were increased by 30%. In set G (circle), let P_{ST} equal to the mean value of P_S, simulating the synchronization between P_{ST} and arterial pressure, as shown in Fig. 4. The slope (E_{max}) of each set is also displayed in Fig. 7.

Fig. 8a shows the fitting result using the clinical data with a parameter vector $\theta = [14.38, 1.24, 0.68, 266.67, 2.97, 162.33, 40.85]$. Normalized F_C and the selected positions of trapezoid vertices are displayed in Fig. 8b. In Fig. 5, at the time of mitral valve closing, the value of P_{LV} is 17 mmHg. Thus the value of P_{LA} was approximately set to 17 mmHg. Given Q_{LV}, P_{LA} and θ, (6) was discretely solved to obtain $\hat{P}_{LV}$. The RMSE between P_{LV} (solid line) and $\hat{P}_{LV}$ (dot) is 2.99 mmHg.

4. Discussion

In the AVP model, dwell times of VC, VR and AC are predetermined. Because of the cumulative error in AVPD, some variables, e.g., s_{AVP} and V_{LV}, cannot numerically converge. A main improvement in the modified model is that the use of $\tilde{c}_{12}$, $\tilde{c}_{45}$ and $\tilde{c}_{56}$ restricts the total system to a limit cycle. In (4), the contribution of LV radial function to flow is equivalent to enlarging A_{LV}. For the same stroke volume, the stroke length of AVP in the modified model is smaller than the one in the original AVP model. In Comparison with the time-varying elastance model, parameters in (6) are constant. The novel modeling method has the potential to be extended to the model-based control of ventricular assist devices.

In Fig. 3, the LV model can be explained by two capacitors in parallel, see (B.8). The dynamics of AVP is represented by an active compliance. The passive compliance is constant, i.e., C_{LV}. Fig. 6 proves that the model is able to characterize the atrioventricular coupling and reproduce common physiological variables. The time-varying elastance model neglects the atrial contraction effect which has been proven crucial to ventricular filling. In our model, the effect is included and the A-wave in mitral flow is acquired. A strong proof supporting the model is that it can reproduce the profile of v_{AVP} and s_{AVP}. The peak of v_{AVP} (7 cm/s) and the stroke length of AVP (1.46 cm) are close to normal physiological values. Moreover, the dicrotic pulse in P_A and the isovolumetric phases in V_{LV} are simulated well. The time-varying elastance model uses an empirical function to fit the PV relationship in the LV chamber, while our model is directly derived from the mechanical structure of left heart.

The value of E_{max} for Set A is 2.09, close to the value of Set B (2.15). A linear ESPVR is approximately satisfied when R_S changes over [0.8, 1.6]. Although parameter perturbations are all set to 30%, their influence on ESPVR appears significant difference. Perturbations in LV parameters (Set C and Set D) lead to larger deviations from the reference value, while the influence of vascular parameters (Set E and Set F) is slight. Moreover, if P_{ST} changes according to certain rules as in Set G, the linear ESPVR is still valid. In clinical studies, since ESPVR is insensitive to changes in afterload and heart rate, it is a measure for cardiac contractility. The property is reproduced by the switched model without any *a priori* knowledge about ESPVR.

From the given θ, the value of C_{LV} is 0.34 ml/mmHg. A_{LV} is 1.8 times larger than A_{LA}. Assuming A_{LV} is 40 cm^2, the value of k_{RAD} is about 1.25. In the condition, L_{AVP} is 32.36 mmHg cm s^2. The ratio between R_{AVP} and L_{AVP} is 14.38. A_1 and A_2 are 5292 mmHg cm^2 and 1318 mmHg cm^2, respectively. The ratio between them is about 4. These values are close to the ones listed in Table 1, implying that the LV parameter values used in simulations match physiological data. In Fig. 8a, P_{LV} is fitted well in terms of RMSE, proving that (6) can reproduce the realistic pressure-flow relationship in the LV chamber. Moreover, these results also prove that the approximation in A_{LV} and k_{RAD} is acceptable in our study.

In the VR phase where F_C is equal to zero, because the E-wave of mitral flow is attributed to the inertia of AVP and the hydraulic force pushing on the piston, the inaccuracy of E-wave measurement will lead to unrealistic estimates of L_{AVP} and A_{LV} /A_{LA}. Therefore, the E-wave data were not used in the fitting procedure. The procedure which only requires the PV loop data during one cardiac cycle is easy to implement for clinical applications. However, at present, the profile of W_1 and W_2 and the estimate of θ are adjusted by a trial method. System identification techniques [33,34] may be helpful to acquire the optimal solution. The robust-

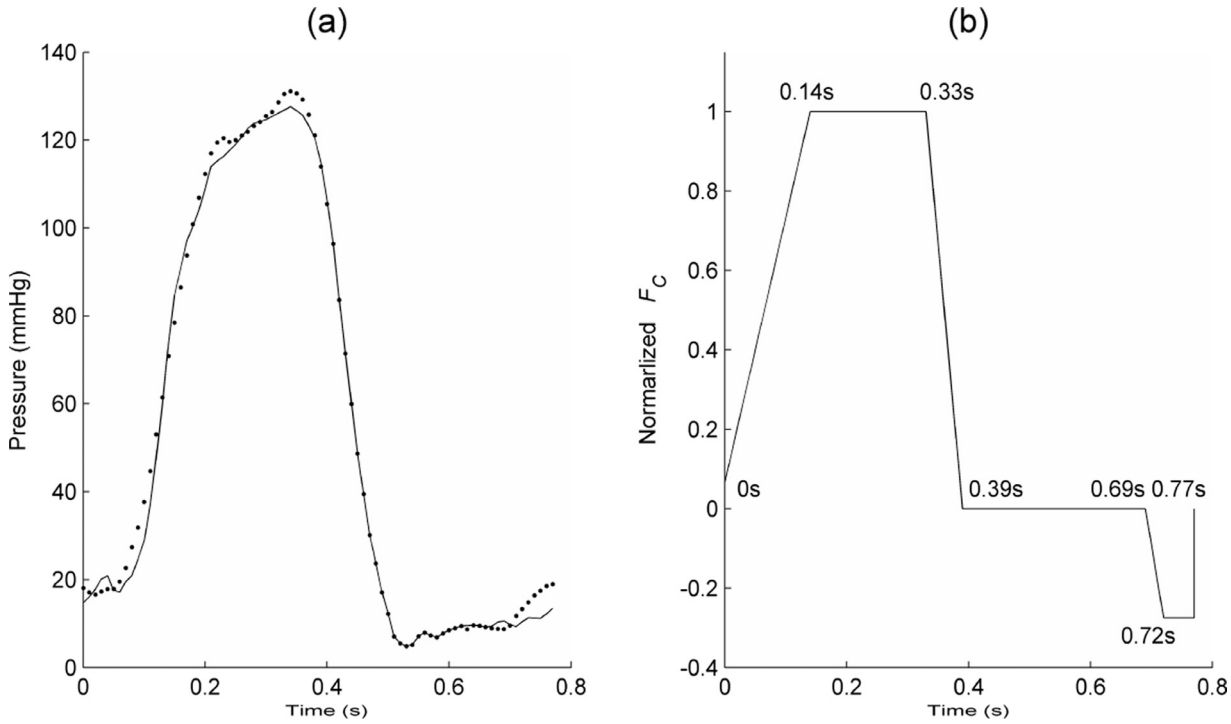

Fig. 8. (a): Comparison between P_{LV} (solid line) and $\hat{P}_{LV}$ (dot) with RMSE = 2.99 mmHg. Note that the estimation errors over the E-wave region were set to zero. (b): Normalized F_C as well as the adjusted positions of trapezoid vertices.

ness of these methods to noise and modeling errors, e.g., the approximation of P_{LA}, should be studied.

There are some other limitations in our study. The simulation of Frank-Starling law where model parameters, e.g., A_1, A_2, A_{LV}, S_{SD}, C_{LV}, may change simultaneously, has not been achieved. The relationship between these parameters should be further studied. The lower measurement accuracy of V_{LV} is a main problem for data fitting. The accuracy can hardly be improved by angiography methods. Other methods, e.g., conductance catheter, should be considered.

5. Conclusions

In this paper, the LV dynamics is modeled based on a modified atrioventricular piston unit. The model is a combination of the longitudinal AVPD and the radial squeezing of LV walls. Through appropriately selecting the state-dependent switching planes, the systemic circulatory system was expressed on a switched system form. An advantage of the method is that the state variables of the system converge to a limit cycle, which will facilitate the analysis of the total system. In simulations, the model is able to characterize the LV hemodynamics and the atrioventricular coupling with a simple structure. A property of the switched model is that the ESPVR with a changing R_S is approximately linear and insensitive to changes in afterload and heart rate. In addition, parameter values of the LV model were validated by clinical data. Experimental results prove that the model can reproduce the realistic pressure-flow relationship in the LV chamber. Parameter values used in the model are within the normal physiological range. Accurate PV loop measurements are required for extending our approach to clinical applications.

Acknowledgments

We gratefully acknowledge the financial support of the National Natural Science Foundation of China (Grant no. 61503167, 61403173 and 61673197) and the Natural Science Foundation of Jiangsu Province, China (Grant no. BK20140240).

Ethical approval

This study was granted by the Ethics Committee and informed consent was obtained from the patient for publication of these data.

Conflict of interest

None declared

Appendix A. Switched linear system

A switched linear system [25,26] can be written on the form

$$\dot{x}(t) = A_{q(t)}x(t) + b_{q(t)}, \tag{A.1}$$

where $x(t) \in \Re^N$ denotes the continuous state vector. $q(t) \in \{1, \ldots, M\}$ denotes the discrete state which indexes the activated subsystem. $A_{q(t)}$ is the system matrix and $b_{q(t)}$ is the input.

A switching point x where a transition between the ith and jth subsystem occurs should satisfy

$$s_{ij}(x) = 0, \tag{A.2}$$

where $s_{ij}(x)$ is a switching law. It can be expressed by a hyperplane in the state space, i.e., $s_{ij}(x) = c_{ij}^T x + d_{ij}$ where c_{ij} is an $N \times 1$ vector and d_{ij} is a constant. A switching plane is defined to be

$$s_{ij}(x) = \tilde{c}_{ij}^T[\tilde{x}^T 1]^T, \tilde{c}_{ij} = [c_{ij}^T d_{ij}]^T. \tag{A.3}$$

If the switch of subsystems forms a closed sequence where each discrete state occurs once and the system maps any switching point onto itself after one cycle of the sequence, a limit cycle which is a closed trajectory in the state space is existent.

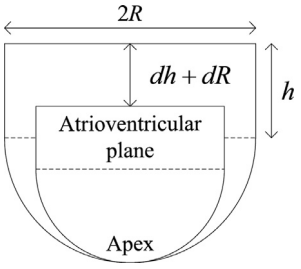

Fig. 9. Illustration of the LV contraction assuming that the outer wall of LV is a hemispherical surface mounted by a hollow cylinder.

Appendix B. LV radial function

For simplicity, assuming that the outer wall of LV is a hemispherical surface with a radius of R mounted by a hollow cylinder with a height of h, as seen in Fig. 9. During the LV contraction, the increment in R and h is dR and dh, respectively. The position of apex remains unchanged over the cardiac cycle. The epicardial volume V_{EC} is

$$V_{EC} = \pi R^2 h + \frac{2}{3}\pi R^3. \tag{B.1}$$

The increment of V_{EC} is equal to

$$dV_{EC} = 2\pi Rh dR + \pi R^2 dh + 2\pi R^2 dR. \tag{B.2}$$

Because the myocardial volume is constant, the increment of LV volume dV_{LV} is equal to dV_{EC} [20].

The atrioventricular plane moves in the longitudinal direction. Because the increment of AVPD is $dh+dR$, the volume change in the longitudinal direction dV_{LON} is

$$dV_{LON} = \pi R^2 (dh + dR). \tag{B.3}$$

The volume change in the radial direction dV_{RAD} is

$$dV_{RAD} = dV_{EC} - dV_{LON} = (2\pi Rh + \pi R^2) dR. \tag{B.4}$$

Assuming the value of h/R is equal to a at the initial position, the flow generated by the radial motion (Q_{RAD}) is

$$\begin{aligned} Q_{RAD} &= \frac{dV_{RAD}}{dt} = (2\pi Rh + \pi R^2)\frac{dR}{dt} \\ &= (2\pi aR^2 + \pi R^2) v_{RAD} \\ &= (2a+1)\pi R^2 v_{RAD} = (2a+1) A_{LV} v_{RAD}. \end{aligned} \tag{B.5}$$

where v_{RAD} is the radial velocity of epicardium and A_{LV} is the epicardial short-axis area of LV.

Adding Q_{RAD} into (3) gives a new equation incorporating both longitudinal and radial motion of LV

$$C_{LV}\dot{P}_{LV} = Q_{LV} + A_{LV} v_{AVP} + Q_{RAD}. \tag{B.6}$$

Substituting (B.5) into (B.6), the equation becomes

$$\begin{aligned} C_{LV}\dot{P}_{LV} &= Q_{LV} + A_{LV} v_{AVP} + (2a+1) A_{LV} v_{RAD} \\ &= Q_{LV} + [1 + \frac{(2a+1) v_{RAD}}{v_{AVP}}] A_{LV} v_{AVP} \\ &= Q_{LV} + (1 + k_{RAD}) A_{LV} v_{AVP}, \end{aligned} \tag{B.7}$$

where $k_{RAD} = (2a+1) v_{RAD}/v_{AVP}$ is an equivalent coefficient representing the contribution of the LV radial function to blood flow. v_{AVP} and v_{RAD} characterize the global function of longitudinal and radial motion of LV, respectively. Because the realistic velocity measurement varies between locations [35], v_{AVP} and v_{RAD} cannot be directly measured. The stroke length of AVP is quite smaller than $h+R$ [21]. Assuming the change in h and R over the cardiac cycle is quite smaller than h and R, respectively, a can be approximately considered to be constant. In (B.7), A_{LV} is also set to be constant. The influence of the approximation in k_{RAD} and A_{LV} to model accuracy should be validated.

From (B.7), $\dot{V}_{LV}/\dot{P}_{LV}$ can be expressed by two capacitors in parallel as follows

$$\begin{aligned} \frac{Q_{LV}}{\dot{P}_{LV}} &= \frac{\dot{V}_{LV}}{\dot{P}_{LV}} = C_{pas} + C_{act} \\ &= C_{LV} - \frac{(1 + k_{RAD}) A_{LV} v_{AVP}}{\dot{P}_{LV}}. \end{aligned} \tag{B.8}$$

The passive compliance (C_{pas}) is equal to C_{LV}. The behavior of AVP is represented by an active compliance (C_{act}) related to v_{AVP} and $\dot{P}_{LV}$.

References

[1] Trayanova NA. Whole-heart modeling: applications to cardiac electrophysiology and electromechanics. Circ Res 2011;108:113–28.
[2] Hunter PJ, Pullan AJ, Smaill BH. Modeling total heart function. Annu Rev Biomed Eng 2003;5:147–77.
[3] Alimohammadi M, Agu O, Balabani S, Díaz-Zuccarini V. Development of a patient-specific simulation tool to analyse aortic dissections: assessment of mixed patient-specific flow and pressure boundary conditions. Med Eng Phys 2014;36:275–84.
[4] Suga H, Sagawa K, Shoukas AA. Load independence of the instantaneous pressure–volume ratio of the canine left ventricle and effects of epinephrine and heart rate on the ratio. Circ Res 1973;32:314–22.
[5] Suga H, Sagawa K. Instantaneous pressure–volume relationships and their ratio in the excised, supported canine left ventricle. Circ Res 1974;35:117–26.
[6] Simaan MA, Ferreira A, Chen S, Antaki JF, Galati DG. A dynamical state space representation and performance analysis of a feedback-controlled rotary left ventricular assist device. IEEE Trans Control Syst Technol 2009;17:15–28.
[7] Wu Y, Allaire PE, Tao G, Olsen D. Modeling, estimation, and control of human circulatory system with a left ventricular assist device. IEEE Trans Control Syst Technol 2007;15:754–67.
[8] Cox LGE, Loerakker S, Rutten MCM, De Mol BAJM, van De Vosse FN. A mathematical model to evaluate control strategies for mechanical circulatory support. Artif Org 2009;33:593–603.
[9] Vandenberghe S, Segers P, Steendijk P, Meyns B, Dion RAE, Antaki JF, et al. Modeling ventricular function during cardiac assist: does time-varying elastance work? ASAIO J 2006;52:4–8.
[10] Arts T, Delhaas T, Bovendeerd P, Verbeek X, Prinzen FW. Adaptation to mechanical load determines shape and properties of heart and circulation: the CircAdapt model. Am J Physiol Circ Physiol 2005;288:H1943–54.
[11] Kuijpers NHL, Hermeling E, Bovendeerd PHM, Delhaas T, Prinzen FW. Modeling cardiac electromechanics and mechanoelectrical coupling in dyssynchronous and failing hearts. J Cardiovasc Transl Res 2012;5:159–69.
[12] Lumens J, Delhaas T, Kirn B, Arts T. Three-wall segment (TriSeg) model describing mechanics and hemodynamics of ventricular interaction. Ann Biomed Eng 2009;37:2234–55.
[13] Arts T, Lumens J, Kroon W, Delhaas T. Control of whole heart geometry by intramyocardial mechano-feedback: a model study. PLOS Comput Biol 2012;8:e1002369.
[14] Lumens J, Ploux S, Strik M, Gorcsan J, Cochet H, Derval N, et al. Comparative electromechanical and hemodynamic effects of left ventricular and biventricular pacing in dyssynchronous heart failure: electrical resynchronization versus left-right ventricular interaction. J Am Coll Cardiol 2013;62:2395–403.
[15] Fritz T, Wieners C, Seemann G, Steen H, Dössel O. Simulation of the contraction of the ventricles in a human heart model including atria and pericardium: finite element analysis of a frictionless contact problem. Biomech Model Mechanobiol 2014;13:627–41.
[16] Seemann F, Pahlm U, Steding-Ehrenborg K, Ostenfeld E, Erlinge D, Dubois-Rande J-L, et al. Time-resolved tracking of the atrioventricular plane displacement in Cardiovascular Magnetic Resonance (CMR) images. BMC Med Imag 2017;17:19.
[17] Hu K, Liu D, Herrmann S, Niemann M, Gaudron PD, Voelker W, et al. Clinical implication of mitral annular plane systolic excursion for patients with cardiovascular disease. Eur Hear J Cardiovasc Imag 2013;14:205–12.
[18] Matos J, Kronzon I, Panagopoulos G, Perk G. Mitral annular plane systolic excursion as a surrogate for left ventricular ejection fraction. J Am Soc Echocardiogr 2012;25:969–74.
[19] Willenheimer R, Cline C, Erhardt L, Israelsson B. Left ventricular atrioventricular plane displacement: an echocardiographic technique for rapid assessment of prognosis in heart failure. Heart 1997;78:230–6.
[20] Carlsson M, Ugander M, Heiberg E, Arheden H. The quantitative relationship between longitudinal and radial function in left, right, and total heart pumping in humans. Am J Physiol Circ Physiol 2007;293:H636–44.
[21] Carlsson M, Ugander M, Mosén H, Buhre T, Arheden H. Atrioventricular plane displacement is the major contributor to left ventricular pumping in healthy adults, athletes, and patients with dilated cardiomyopathy. Am J Physiol Circ Physiol 2007;292:H1452–9.
[22] Arutunyan AH. Atrioventricular plane displacement is the sole mechanism of atrial and ventricular refill. Am J Physiol Circ Physiol 2015;308:H1317–20.

[23] Maksuti E, Carlsson M, Arheden H, Kovács SJ, Broomé M, Ugander M. Hydraulic forces contribute to left ventricular diastolic filling. Sci Rep 2017;7:43505.
[24] Maksuti E, Bjällmark A, Broomé M. Modelling the heart with the atrioventricular plane as a piston unit. Med Eng Phys 2015;37:87–92.
[25] Rubensson M, Lennartson B. Global convergence analysis for piecewise linear systems applied to limit cycles in a DC/DC converter. In: Proceedings of the 2002 American Control Conference (IEEE Cat. No.CH37301), 2. IEEE; 2002. p. 1272–7.
[26] Rubensson M, Lennartson B. Stability of limit cycles in hybrid systems using discrete-time Lyapunov techniques. In: Proceedings of the Thirty-ninth IEEE Conference on Decision and Control (Cat. No.00CH37187), 2. IEEE; 2000. p. 1397–402.
[27] Shu Z, Lam J, Xiong J. Static output-feedback stabilization of discrete-time Markovian jump linear systems: a system augmentation approach. Automatica 2010;46:687–94.
[28] Lin H, Antsaklis PJ. Stability and stabilizability of switched linear systems: a survey of recent results. IEEE Trans Autom Control 2009;54:308–22.
[29] Goldberger AL, Amaral LAN, Glass L, Hausdorff JM, Ivanov PC, Mark RG, et al. PhysioBank, PhysioToolkit, and PhysioNet: components of a new research resource for complex physiologic signals. Circulation 2000;101:E215–20.
[30] Johnson AEW, Pollard TJ, Shen L, Lehman LH, Feng M, Ghassemi M, et al. MIMIC-III, a freely accessible critical care database. Sci Data 2016;3:160035.
[31] Cingolani OH, Kass DA. Pressure–volume relation analysis of mouse ventricular function. Am J Physiol Circ Physiol 2011;301:H2198–206.
[32] Kass DA, Maughan WL, Guo ZM, Kono A, Sunagawa K, Sagawa K. Comparative influence of load versus inotropic states on indexes of ventricular contractility: experimental and theoretical analysis based on pressure–volume relationships. Circulation 1987;76:1422–36.
[33] Huang H, Yang M, Zang W, Wu S, Pang Y. In vitro identification of four-element Windkessel models based on iterated Unscented Kalman filter. IEEE Trans Biomed Eng 2011;58:2672–80.
[34] Huang H, Yang M, Wu S, Liao H. Dynamic modeling of the outlet of a pulsatile pump incorporating a flow-dependent resistance. Med Eng Phys 2013;35:1097–104.
[35] Petersen SE, Jung BA, Wiesmann F, Selvanayagam JB, Francis JM, Hennig J, et al. Myocardial tissue phase mapping with cine phase-contrast MR Imaging: regional wall motion analysis in healthy volunteers. Radiology 2006;238:816–26.